Transfer hydrogenation of furfural to furfuryl alcohol over modified Zr-based catalysts using primary alcohols as H-donors

Yantao Wang, Deyang Zhao, Rui Liang, Konstantinos S. Triantafyllidis, Weiran Yang, Christophe Len

Transfer hydrogenation of furfural to furfuryl alcohol over modified Zr-based catalysts using primary alcohols as H-donors

Yantao Wang[a,b], Deyang Zhao[b,c], Rui Liang[d], Konstantinos S. Triantafyllidis[e,f], Weiran Yang[a] and Christophe Len[b*]

[a] Nanchang University, School of Resources Enviromental & Chemical Engineering, 330031, Nanchang, China
[b] ChimieParisTech, PSL Research University, CNRS, Institute of Chemistry for Life and Health Sciences, 11 rue Pierre et Marie Curie, F-75005 Paris, France.
[c] School of Chemistry and Materials Science, Ludong University, Yantai 264025, China.
[d] Anhui Agricultural University, School of Resources and Environment, No 130 Changjiang west road, Heifei, Anhui, China
[e] Department of Chemistry, Aristotle University of Thessaloniki, University Campus, P.O. Box 116, GR-54124 Thessaloniki, Greece
[f] Chemical Process & Energy Resources Institute, CERTH, Thermi P.O. Box 60361, GR-57001 Thessaloniki, Greece
E-mail address: christophe.len@chimieparistech.psl.eu (C. Len)

Abstract: Catalytic transfer hydrogenation is gaining increasing attention as a promising alternative to conventional hydrogenation with H_2. In present work, a series of modified Zr-based catalysts were synthesized and tested for furfural catalytic transfer hydrogenation into furfuryl alcohol (FA). The results indicated that more than 13% of furfural conversion and furfuryl alcohol yield could be achieved with modified zirconium hydroxide (mZrH) at 140 °C when compared with zirconium hydroxide (ZrH) using ethanol as H-donor and solvent in continuous flow regime, and the activity could be further enhanced by increasing the reaction temperature or Ru loading on the catalyst. The best result of 92 % furfural conversion with ~99 % FA selectivity was obtained at 150 °C with 6% Ru/mZrH as catalyst, and the productivity

of FA is 5.5 mmol g^{-1} h^{-1} which is 2 times higher than that reported with ZrH in batch. Moreover, long-term stability study of the catalysts indicated that 6% Ru/mZrH not only performs a better activity, but also a better stability than 6% Ru/ZrH. Characterizations of the catalysts by BET, XRD, EA, IR, SEM-EDS, XPS and CO_2 adsorption indicated that zirconium hydroxide (ZrH) was successfully modified with hydroxylamine, leading to significantly change of its morphology and basic sites. And the deactivation of the catalysts was due to both the leaching of Ru and the deposition of side-products on its surface.

Keywords: Furfural, Furfuryl alcohol, Green chemistry, Continuous flow, Heterogeneous catalyst

1. Introduction

Nowadays, with the depletion of fossil fuel resources and environmental concerns, biomass valorization is becoming one of the most appealing research topics in the context of sustainable chemistry [1]. Each year, more than 170 billion metric tons of lingocellulosic biomass is produced by photosynthesis, means that biomass is a suitable and available carbon source for chemical synthesis that could alleviate the problems caused by vast consumption of fossil fuels [2,3]. Furfural, one of the top 30 bio-based platform molecules, can be obtained by acid-catalyzed hydrolysis and dehydration of hemicellulose, or be generated in bio-oil by fast pyrolysis of biomass [4,5]. Derived from furfural, various chemicals could be produced, such as furfuryl alcohol (FA), tetrahydrofurfuryl alcohol (THFA), 2-methylfuran (MF), 2-methyltetrahydrofuran (MTHF), as well as cyclopentanone, olefins etc. [6-11]. Among them, the most popular product is FA, as approximately 60–62% of global

production of furfural is converted into FA, which mainly used for the production of thermostatic resins, liquid resins for strengthening ceramics, as well as for the production of various synthetic fibers, rubbers-resins and farm chemicals [12-14], besides, it can be also employed for the manufacture of lysine, vitamin C, lubricants, dispersing agents and plasticizers etc [15].

Over the past five decades, FA is industrially produced with copper chromite (Cu-Cr) catalyst in batch conditions [16]. The main drawbacks of this process are the high toxic nature of chromium oxides and the moderate activity in furfural conversion. Moreover, the relative harsh reaction conditions (180 ^{o}C, 7-10 MPa H_2) and easy deactivation of the catalyst in vapor phase, impelled researchers to develop Cr free catalytic system for the production of FA from furfural [9, 17-19]. Some efforts have been devoted on the synthesis of different kinds of catalysts, including noble metal Au [20], Ru [21-23], Pt [24-26], Pd [27-30], non-noble metal Cu [15,17,31,32], Ni [33-36] and Co [37] as well as bimetallic catalysts [38] supported on different materials. On the other hand, even vapor phase hydrogenation of furfural was adopted in most cases, liquid phase hydrogenation seems more economic as no requirement for furfural vaporization, that's why it is frequently employed in some countries, e.g in China [37,39]. Moreover, the hydrogenation of furfural was mostly performed at high pressure, which will cause security problems, for example, leakage of reactants, storage of hydrogen, explosion of reactor, etc. To avoid these disadvantages, a promising alternative to the classical catalytic hydrogenation is transfer hydrogenation *via* Meerwein, Ponndorf and Verley (MPV) process. Very recently, catalytic transfer hydrogenation of furfural to FA has been investigated over Pd/Fe_2O_3 [27], Cu/Mg/Al [40,41], $Cu/MgO-Al_2O_3$ [42], $Cu/AC-SO_3H$ [43], γ-Al_2O_3 [44] and γ-Fe_2O_3@HAP [45] catalysts. In 2016, Hao et al. found that low-cost

$ZrO(OH)_2$ showed a good catalytic transfer hydrogenation of 5-hydroxymethyl furfural (HMF) at 150 °C [46]. Later, Zhang et al. found that $Zr(OH)_4$ presented excellent transfer hydrogenation ability to produce FA from furfural, and the experiment gave 99 % of FA yield at 170 °C for 2.5 h while using iso-propanol as H-donor and solvent, however, a poor furfural conversion (59 %) and FA yield (39 %) were attained with ethanol [47]. Generally, catalytic transfer hydrogenation using primary alcohols, such as ethanol, will be more appealing, because ethanol is more accessible from biomass, and further conversion of FA into other high value-added compounds, such as ethyl levulinate (EL), γ-valerolactone (GVL) could be achieved without the separation of FA in ethanol (Scheme 1).

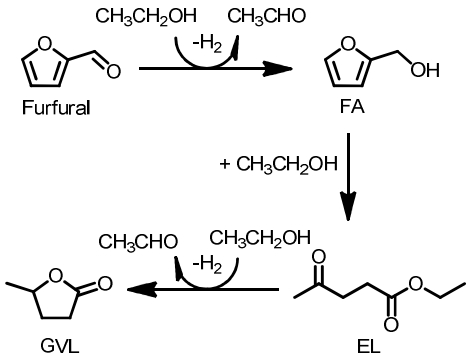

Scheme 1. The formation and conversion of furfuryl alcohol in ethanol.

Therefore, we herein synthesized a series of Zr-based catalysts, and tested their activity for furfural selective transfer hydrogenation to FA in continuous flow with primary alcohols as H-donors. To the best of our knowledge, there has been no report so far on the modification of ZrH with hydroxylamine. The catalysts were carefully characterized, and their catalytic performance and stability were systematically investigated. In a word, the novelty of this work includes: 1) developed a new modified Zr-based catalyst; 2) realized liquid phase furfural

transfer hydrogenation in continuous flow; 3) applied bio-based primary alcohols as H-donners instead of fossil-based 2-propanol, which respects better to sustainable chemistry.

2. Materials and methods

2.1. Materials

Furfural (>99 %), furfuryl alcohol (>98 %) and decane (> 99%) were purchased from Acros Organic. Zirconium (IV) chloride (> 99 %), ruthenium(III) chloride (Ru content 45-55%), sodium borohydride (> 98 %), sodium hydroxide anhydrous (97 %) and hydroxylamine hydrochloride (98%) were supplied by Sigma Aldrich. Methanol, ethanol, 1-propanol, 1-butanol and *N*,*N*-dimethylformamide anhydrous (> 99 %) were furnished from Fisher Scientific. All the chemicals were used as received without further purification or treatment. The water used in all experiments was a Millipore Milli-Q grade.

2.2. Catalyst preparation.

Zirconium hydroxide (ZrH). First, zirconium (IV) chloride (3.455 g) was dissolved in *N*,*N*-dimethylformamide (90 mL), and then aqueous solution of sodium hydroxide (1 M) was added dropwise to regulate the pH value to 7 under vigorous agitation. The resulting precipitate was thoroughly washed with deionized water several times. The precipitate was dried at 333 K overnight and was further ground to obtain ZrH powder.

Modified Zirconium hydroxide (mZrH). First, zirconium (IV) chloride (3.455 g) was dissolved in *N*,*N*-dimethylformamide (90 mL), and then mol equivalent hydroxylamine hydrochloride solution in *N*,*N*-dimethylformamide (30 mL) was dropwisely added into the solution above while heated at 60 °C for 24 h under

vigorous agitation, followed by adding aqueous solution of sodium hydroxide (1 M) to regulate the pH value to 7. The resulting precipitate was thoroughly washed with deionized water several times. The precipitate was dried at 333 K overnight and was further ground to obtain mZrH powder.

6% *Ru/ZrH*. First, zirconium (IV) chloride (3.455g) was dissolved in *N*,*N*-dimethylformamide (90 mL), then ruthenium(III) chloride (0.29 g) (theoretical Ru loadings 6 wt%) with water (1 mL) were added into the solution above under vigorous agitation for 24 h, followed by regulating the pH value to 7 with aqueous solution of sodium hydroxide (1 M), and then a freshly made $NaBH_4$ solution ($NaBH_4$-Ru, 5:1, mol/mol) was added dropwise to reduce Ru^{3+} to Ru^0. The black precipitate was thoroughly washed with deionized water several times and dried at 333 K overnight and was further ground to obtain 6% Ru/ZrH powder.

2-6% Ru/mZrH. First, zirconium (IV) chloride (3.455g) was dissolved in *N*,*N*-dimethylformamide (90 mL), then mol equivalent hydroxylamine hydrochloride solution in *N*,*N*-dimethylformamide (30 mL) was dropwisely added into the solution above while heated at 60 °C for 24 h under vigorous agitation. Then different amount of ruthenium(III) chloride with water (1 mL) were added into the solution above under vigorous agitation for 24 h, followed by regulating the pH value to 7 with aqueous solution of sodium hydroxide (1 M), and then a freshly made $NaBH_4$ solution ($NaBH_4$-Ru, 5:1, mol/mol) was added dropwise to reduce Ru^{3+} to Ru^0. The black precipitate was thoroughly washed with deionized water several times and dried at 333 K overnight and was further ground to obtain 2-6% Ru/mZrH powder.

2.3. *Catalytic reaction*

The experiments in primary alcohols were conducted in a H-Cube Pro Flow Reactor (ThalesNanoTM, Hungary), which could supply a continuous H_2 flow

produced from the electrolysis of water to the central reactor module in which a 30 mm CatCart was installed, corresponding with reactor volumes of 0.38 mL. The corresponding total flow through volumes (including feed lines, reactor and product lines) were 5.0 mL. In this work, no hydrogen mode was used. A filter was installed in the entrance of the pump to avoid undissolved compounds entering the system. First, pure solvent was pumped through the system before reaching the set temperature (140-150 °C) and pressurization (20 bar). Once the reaction conditions were stable, the pure solvent feed was changed to the 0.2 M furfural feedstock (internal standard: decane). And the first sample (time zero) was collected after 10 mL furfural feedstock was pumped. Further samples were collected after regular time interval (30 min).

2.4. *Product analysis*

The collected samples were analyzed on a GC-FID gas chromatograph (HP, 14009 Arcade, New York, United States) coupled with a FID detector equipped with a Supelco 2-8047-U capillary column (30 m x 0.25mm i.d. and 0.1 μm film thickness, Alltech Part No.31163-01). N_2 was used as carrier gas at a rate of 1 mL min^{-1}. The temperature of the injector was set 250 °C and the oven started at 80 °C, held for 5 min, raised to 100°C at a rate of 10°C min^{-1}, held for 5 min. and then raised to 120 °C at a rate of 10°C min^{-1} and held for 10 min at 120 °C. The ionisation mode was FID (70 eV, 300 μA, 250 °C). The identification of the compounds was performed by comparison of the retention times with pure standards.

The furfural (F) conversion and the selectivity and the yield of each hydrogenation product (P) in continuous flow experiments were calculated as the following:

$$Conversion\ \ F\ \ (mol\%) = \frac{[CF_{Initial} - CF_{Final}]}{C\ \ F_{Initial}} \times 100$$

$$Yield\ \ P\ \ (mol\%) = \frac{CP}{CF_{Initial}} \times 100$$

$$Selectivity\ \ (\%) = \frac{Yield\ \ P}{Conversion\ \ F}\ \ \times 100$$

$$Productivity(mmol * g^{-1} * h^{-1}) = \frac{CF_{Initial} \times FR \times Yield\ \ P}{m_{cat.loading}}\ \ \times 100$$

CF and CP are the concentrations of furfural and hydrogenation product (mol mL^{-1}), FR means the flow rate. We have assumed that the total volume in the flow experiments kept constant (no evaporation loss).

Nitrogen adsorption/desorption experiments at -196 °C were performed for the determination of specific surface area (multi-point BET method), total pore volume (at P/Po = 0.99), micropore area by t-plot analysis and pore size distribution (BJH method using adsorption data or DFT analysis) of the samples which were previously outgassed at 150 °C for 16 h under $5x10^{-9}$ Torr vacuum, using an Automatic Volumetric Sorption Analyzer (Autosorb-1MP, Quantachrome). Fig. S1 shows the nitrogen adsorption-desorption isotherms recorded for the different catalysts synthesized in this work.

Powder XRD experiments were conducted on a Shimadzu X-ray 7000 diffractometer using a CuKα X-ray radiation operating at 45 kV and 100 mA; counts were accumulated in the range of 5-75º with 0.02º steps (2θ) with counting time 2 s per step.

The XPS measurements were carried out with a Phi Quantera Scanning X-ray Microprobe instrument using Al Kα (h·ν=1486.7 eV) radiation at Chevron Energy Technology Company in Richmond (CA), USA. The instrument is equipped with a hemispherical energy analyzer with multichannel detection and an energy resolution

of 1.1 eV. The catalysts were mounted on double-sticky tape confining an area of approximately 0.8 cm x 0.8 cm. The tape was completely covered by the catalyst powder and the sample surface was carefully smoothed. Spectra were collected for C-1s, O-1s, N-1s, Zr-3d and Ru-3p photoelectron peaks. Total spectral accumulation times were 100 minutes per analysis area while irradiating with 100 W of X-ray irradiation. The binding energies (BE) were referenced to the C-1s peak (284.4 eV) to account for charging effects.

SEM-EDS analysis of the catalysts at different stage of the experiments was performed on a Quanta FEG 250 (FEI) equipped with a microanalysis detector for EDX (Brucker). SEM micrographs acquired in secondary electron mode were obtained at low vacuum, 15 kV of accelerating voltage with a 10 mm working distance. EDX spectra were collected at 30° angle, 15 kV accelerating voltage and 10 mm working distance.

FTIR spectra were recorded on a Perkin-Elmer SPECTRUM 2000 FTIR instrument in the range of 400-3700 cm^{-1}.

Carbon and nitrogen were analyzed with an Elemental Vario EL Cube. The analysis was conducted according to BS EN 15104 (2011).

CO_2 pulse adsorption was performed on an Adsorption-Desorption Analyzer (Hunan, Huasi). Catalyst samples were pretreated at 333 K in a N_2 flow (30 mL min^{-1}, Jiangxi Hongwei) for 2 h. Then the basicity of catalysts was measured by CO_2-titration at 333 K.

3. Results and discussion

3.1. Characterizations of catalyst

The porosity characteristics (from N_2 sorption experiments) of Zr-based catalysts are shown in Table 1. ZrH is a micro/mesoporous material with a low contribution of microporosity. About 77 % of its total surface area and 87 % of its total pore volume is attributed to meso/macropores, the rest being attributed to micropores. However, despite of the total surface area decreased 16 % after modification (compared to ZrH), mZrH possesses a higher contribution of microporosity, as the micropores took up 56 % of its total surface area and 37 % of its total pore volume, and the meso/macropores decreased accordingly. No significant changes of the total and micropore surface area, as well as the pore volumes were observed with Ru loading. The N_2 isotherm shapes (Fig. S1 in the Supporting Information) indicated that all of Zr-based materials were characteristic of IV isotherm with a H_2 hysteresis loop, which is in line with the literature report [41]. Besides, both of BJH and DFT method were used to evaluate the pore size distribution of these materials, but no distinct peaks for mZrH catalysts in the BJH pore size distribution curves were observed, however, apparent peaks at ~2.5 nm were observed for ZrH based catalyst (Fig. S2 in the Supporting Information), which can be explained as the BJH method is only valid for mesoporous materials, i.e. for pore diameters equal and larger than ca. 2.0 nm. On the other hand, the DFT method is being used more often today, covering the whole range. As expected, peaks were found for mZrH catalysts in 1.8-3.3 nm and for ZrH catalysts, the range is 2.1-4.6 nm in the DFT pore size distribution curve (Fig. S3). Table 1 also revealed that the total surface area of the spent 6% Ru/ZrH and 6% Ru/mZrH decreased 21 % and 16 % respectively, indicated that deposition of side-products on the catalysts

surface maybe occurred, which was probably responsible for the deactivation of the catalysts.

Table 1

Porosity and crystal size data of Zr-based catalysts.

Catalyst	Total SSA (m^2/g) [a]	Total pore volume (cc/g) [b]	Micropore area(m^2/g) and volume (cc/g) [c]	Meso/macro- pore & external area (m^2/g) and volume (cc/g) [d]
ZrH	308	0.23	70 / 0.03	238 / 0.20
mZrH	257	0.16	143 / 0.06	114 / 0.10
6%Ru/ZrH	352	0.34	67 / 0.03	285 / 0.31
6%Ru/mZrH	221	0.14	101 / 0.04	120 / 0.10
6%Ru/ZrH[e]	277	0.28	15/ 0.002	262 / 0.28
6%Ru/mZrH[e]	186	0.11	100/ 0.04	86 / 0.07

[a] SSA: specific surface area from N_2 sorption at -196 °C (multi-point BET method).
[b] Total pore volume at $P/P_o = 0.99$.
[c] t-plot method.
[d] Meso/macropore & external area = Total SSA - Micropore area; Meso/macropore volume = Total pore volume - Micropore volume (t-plot).
[e] spent catalysts, recovered from long-term stability study, reaction conditions: 150 ºC, 0.2 M Furfural, 20 bar dynamic pressure, catalyst (0.6 g) and 0.3 mL min^{-1} flow rate, 300 min.

The catalysts were also characterized using powder XRD analysis and the respective patterns (Fig. 1). Interestingly, all the Zr-based catalysts exhibited similar patterns with two broad and weak peaks in an angle range from 25 to 60°, suggesting that the samples were characteristic of an amorphous structure. Noting that no characteristic peaks due to ZrO_2 or Ru metallic or other nature were found, indicating that Ru is very well dispersed on the support. And the spent catalysts presented similar patterns with fresh catalysts implying that no new phase formed after long-term stability study.

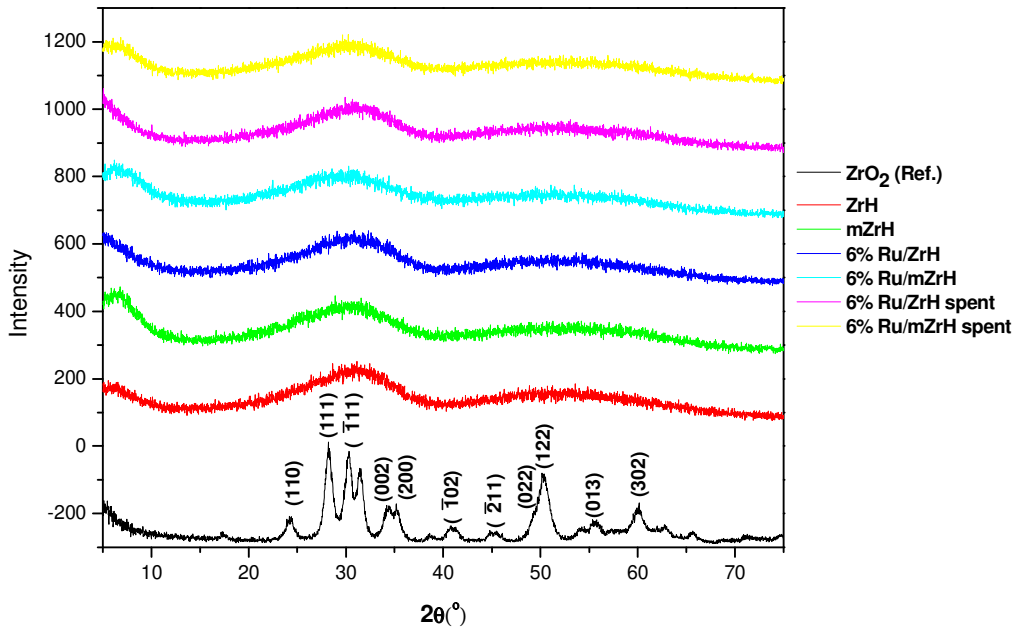

Fig. 1. XRD patterns of Zr-based catalysts.

Meanwhile, as shown in SEM images, the morphology of 6% Ru/ZrH and 6% Ru/mZrH particles remains unchanged after recycle (Fig. 2). The "bright points" points in the Ru mapping images, is probably due to very few Ru aggregates; otherwise, Ru is homogeneously dispersed in the particles. To gain more insights to the deactivation of spent catalyst, point EDS was also performed, and the results were shown in Table S1. One can notice that Ru is leached from both catalysts (not to such a high extent), which means that the leaching of Ru also attribute to the deactivation of the catalysts. And EDS data also revealed that the leaching of Ru, Na etc. attributed to the fact that the relative higher Zr content of in the spent catalysts than that in fresh ones.

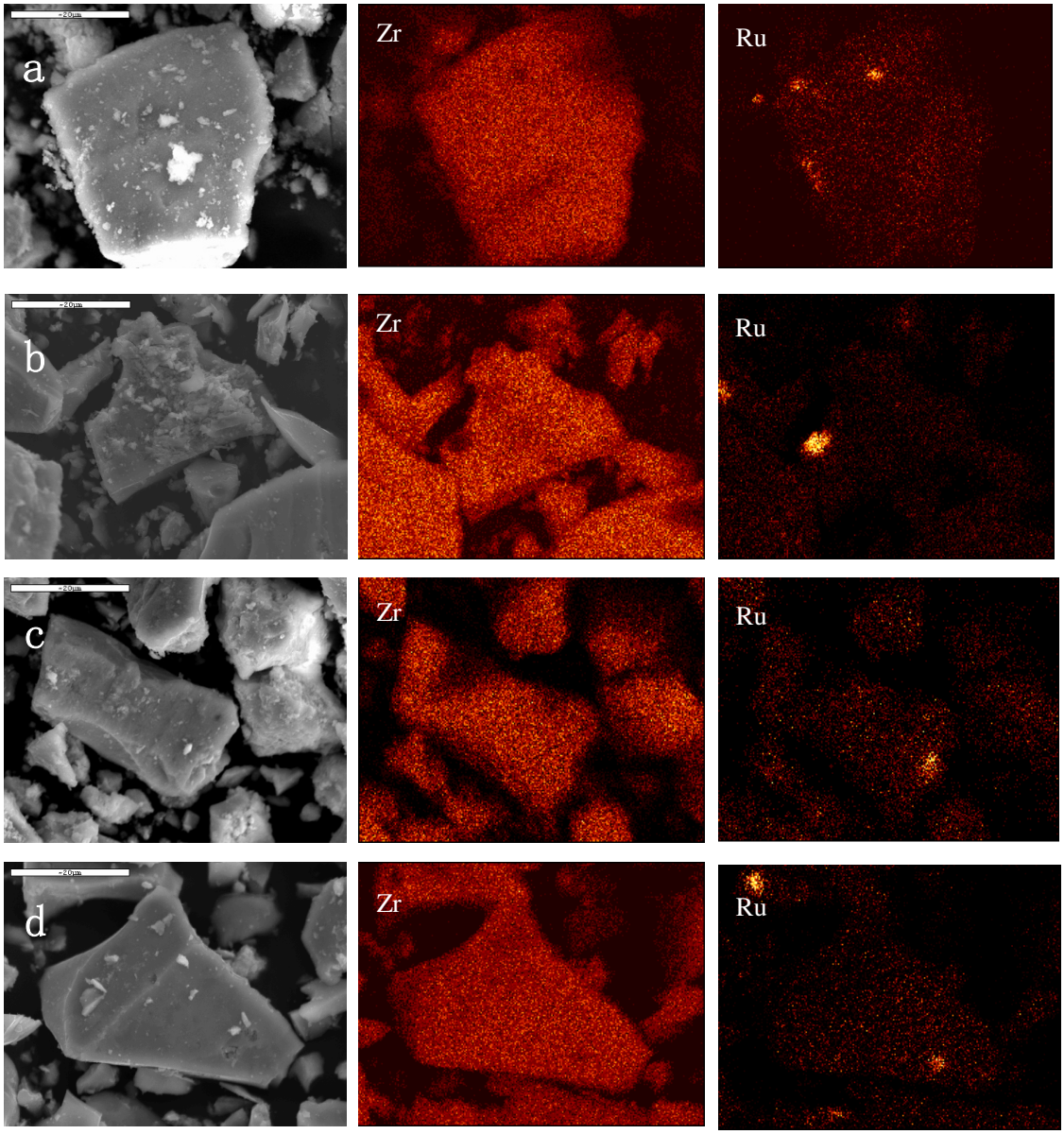

Fig. 2. SEM images and elemental mapping of Zr and Ru for a. 6% Ru/ZrH; b. 6% Ru/mZrH; c. 6% Ru/ZrH spent; d. 6% Ru/mZrH spent. (spent catalysts were recovered from long-term stability study as mentioned in Table 1)

In order to gain more insight to the structure of the catalysts, FT-IR and elemental analysis were also performed. The FT-IR spectra (Fig. S4) showed that the broad band at 3400 cm^{-1} is due to the stretching vibration of the hydroxyl group in ZrH and mZrH. It is clearly to see that mZrH has lower hydroxyl group content than ZrH. The band at 1624 cm^{-1} may be assigned to the scissor bending mode of molecular water,

and to O–C–O stretching modes of CO_2 interacted with terminal OH groups of ZrH [40]. Zhang and Hao et al. suggested that the interactions of CO_2 on the surface of ZrH leading to three kinds of basic sites (Fig. 3a-c), and the interactions of NH_3 on the surface of ZrH formed two kinds of acid sites (Fig. 3d and 3e) [40,41]. The relative unnoticeable band at 1624 cm^{-1} in mZrH indicated that its basic sites are less than that in ZrH. Moreover, the medium basic sites at the band 1345 cm^{-1}, which was attributed to bidentate carbonates (Fig. 3b) showed the same tendency. To confirm this conjecture, CO_2 pulse adsorption was carried out to measure the basic sites of ZrH and mZrH. The results showed that the basic sites of ZrH is more than 10 times than mZrH (650μl CO_2 adsorption/gZrH *vs* 52μl CO_2 adsorption/g_{mZrH}), which is in accordance with our FT-IR results. On the other hand, no acid sites derivate from the interaction between ZrH and NH_3 in our case, because ZrH was prepared by precipitation method with sodium hydroxide rather than aqueous ammonia. The most important is to understand that how hydroxylamine modified zirconium. According to literature, hydroxylamine could act as ligand forming complex with metal ions, which has linkage isomerism ($HOH_2N\rightarrow M$ and $H_3NO\rightarrow M$) [48]. Therefore, we supposed that Zr^{4+} firstly formed complex with hydroxylamine [$(HOH_2NZr)^{4+}$ or $(H_3NOZr)^{4+}$], and then neutralized by sodium hydroxide solution, and maybe further interact with CO_2 in air. In our case, we preferred the complex $(H_3NOZr)^{4+}$ formed rather than $(HOH_2NZr)^{4+}$ as lower OH band intensity was observed in mZrH.

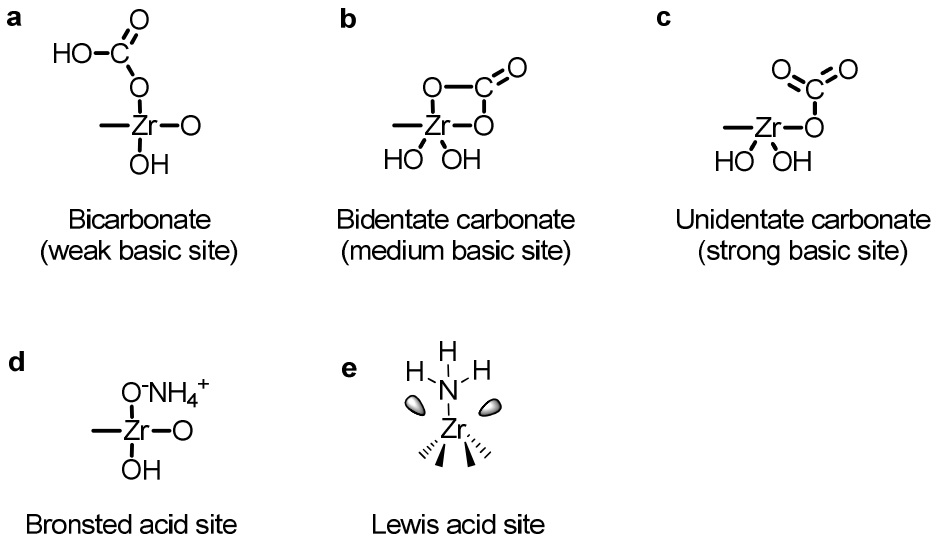

Fig. 3. Acid and basic sites on the surface of ZrH.

To make clearer about hydroxylamine modification on ZrH, here, we did the elemental analysis of 'N' and 'C' (Table 2). Apparently, without modification, no 'N' element was found in ZrH, fresh and spent 6% Ru/ZrH, but more than 3 % of 'C' was detected in fresh catalyst, which confirmed the interaction of CO_2 with these materials, and a little higher 'C' content in the spent 6% Ru/ZrH suggested some carbonaceous deposit on the catalyst after reaction. Gratifyingly, the elemental analysis showed that the modified samples contain 'N', meaning that hydroxylaomine has been successfully introduced into ZrH. The relatively higher value for the 6% Ru/mZrH compared to the parent mZrH could be attributed to inhomogeneous distribution of 'N' amongst the particles. It is encouraging that 'N' element stays after reaction, which possibly benefit to its superior stability than ZrH. However, the higher 'C' content in spent 6% Ru/mZrH suggested that some active sites covered by side-products (such as oligomers derived from FA) leading to the decrease of surface area (BET analysis) and the loss of activity.

Table 2

Elemental analysis of Zr-based catalysts.

Catalyst	Element	
	N (wt.%)	C (wt.%)
ZrH	0.0	3.8
6% Ru/ZrH	0.1	3.2
6% Ru/ZrH spent	0.0	6.5
mZrH	0.7	5.8
6% Ru/mZrH	2.1	4.2
6% Ru/mZrH spent	0.7	7.0

Spent catalysts were recovered from long-term stability study as mentioned in Table 1

XPS characterization was also carried out to get more clues that if hydroxylamine has been successfully modified on the surface of ZrH. Fig. 4a illustrated the full range XPS spectra of 6% Ru/ZrH and 6% Ru/mZrH, and Fig. 4b-d presented the high-resolution scans of the XPS spectra of O1s, N1s and Zr3d, respectively. Clearly, Fig. 4c depicted that 'N' was successfully introduced into 6% Ru/mZrH, and the binding energy was ~401 eV. Moreover, two surface species with binding energies of 530.4 and 531.8 eV for 6% Ru/ZrH in the high-resolution of O1s spectra (Fig. 4b) were characteristic of ZrO_2 and Zr-OH, respectively. This means that ZrH might actually existed in the form of $ZrO(OH)_2 \cdot xH_2O$, which is well-consisted with the literature [41]. It is noteworthy that the third species with binding energy of 532.2 eV in O1s spectra for 6% Ru/mZrH could be due to O-NH_3 group. And in terms of Zr3d spectra (Fig. 4d), the binding energies of 181.8 eV and 184.2 eV confirmed the presence of Zr^{4+} species in ZrO_2 and Zr-OH.

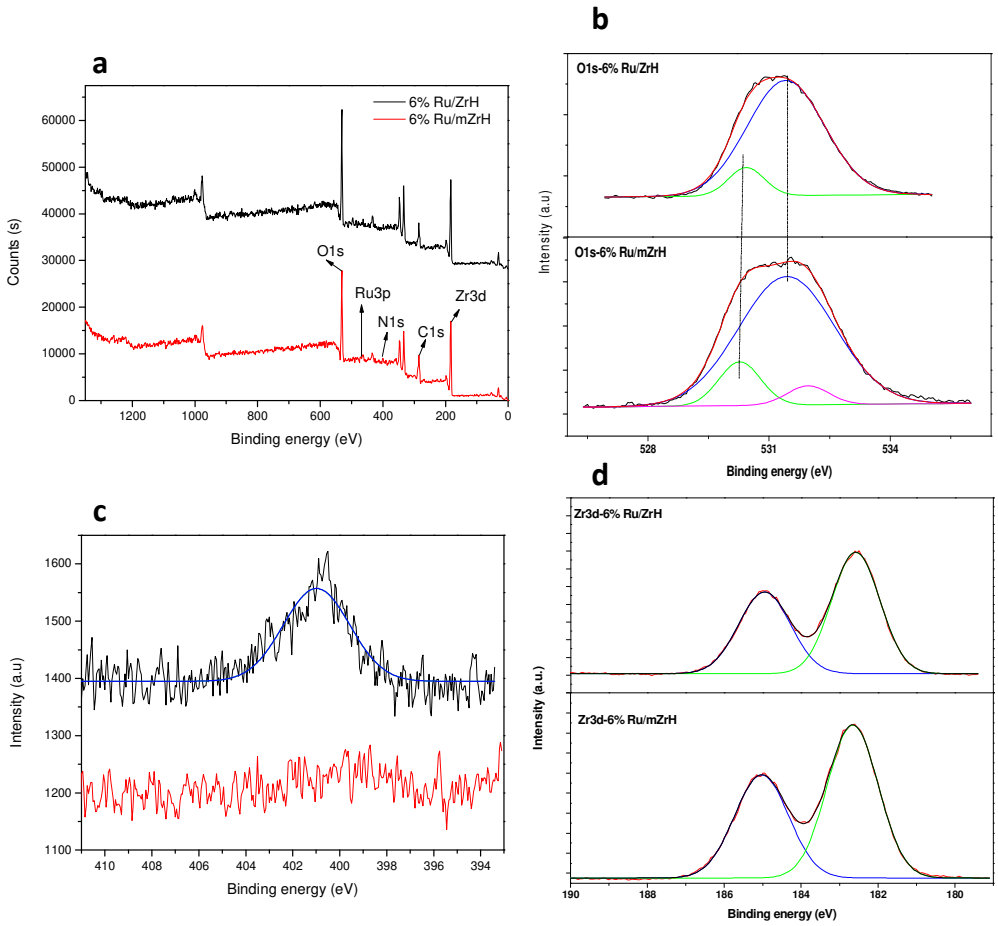

Fig. 4. XPS characterization of 6% Ru/ZrH and 6% Ru/mZrH: (a) full spectra; (b) O1s; (c) N1s and (d) Zr3d.

3.2. Catalytic transfer hydrogenation of furfural to FA in continuous flow

In this section, furfural transfer hydrogenation over a series of catalysts was tested in continuous flow regime to compare their catalytic activity. Then, different primary alcohols as H-donors were screened, and long-term stability of the selected catalysts was also studied to further reveal the influence of hydroxylamine modification on the catalyst performance.

The catalytic activity of synthesized Zr-based catalysts for the transfer hydrogenation of furfural was tested in continuous flow. First, the experiment was conducted at 140 ^{o}C with 0.2 M furfural, 0.6 g catalyst loading and 0.3 mL min^{-1} flow

rate. Ethanol was initially chosen as both the solvent and H-donor with 20 bar dynamic pressure to make sure that the reaction was carried out under liquid phase. ZrH without modification gave 67% of FA yield with 72 % furfural conversion (Table 3, entry 1), and mZrH improved FA yield to 77 % with 81 % of furfural conversion (Table 3, entry 2). As expected, furfural conversion gradually increased from 82 % to 86 % and FA yield increased from 79 % to 84 % with the loading of Ru from 2 wt% to 6 wt%, and the selectivity of FA was also improved (Table 3, entries 4, 5 and 7). Herein, it should be noted that in these cases the only byproduct detected was 2-furanacrolein (Scheme 2, identified by GC-MS), which formed by aldol condensation between furfural and acetaldehyde derived from ethanol.

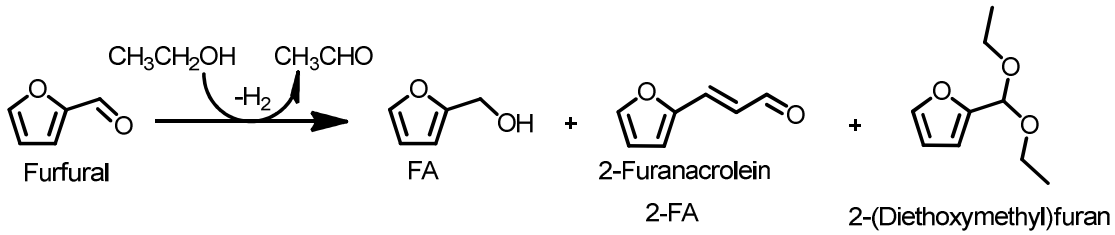

Scheme 2. Furfural transfer hydrogenation pathway in ethanol.

When the reaction temperature goes up to 150 ^{o}C, the conversion of furfural increased gradually, while FA yield and selectivity increased more intensely especially with 6 % Ru/mZrH (Table 3, entry 8). More catalyst loading led to a higher furfural conversion and FA yield, however the productivity of FA decreased from 5.5 to 3.8 mmol g^{-1} h^{-1} (Table 3, entries 8 and 9). It is noteworthy that continuous flow regime is superior than batch as a better FA yield and productivity were achieved with ZrH (Table 3, entry 1 *vs* entry 13) even at lower reaction temperature (140 ^{o}C *vs* 150 ^{o}C). The result of entry 10 indicated that the active species of Ru is metallic Ru^{0} rather than Ru^{3+} ions. Interestingly, 3 % of 2-(diethoxymethyl)furan was measured

with non-reduced 6% $RuCl_3$/mZrH as catalyst, which is possibly attributed to the Lewis acid nature of Ru^{3+} (Table 3, entry 10). 6 % Ru/ZrH offered a better FA yield and selectivity with a higher furfural conversion than ZrH, but it is inferior to that obtained with 6 % Ru/mZrH under identical conditions (Table 3, entries 1 and 11). When compared with literatures, herein, we got a better FA productivity with ethanol as both H-donor and solvent, and the result is comparable to that obtained with 2-propanol as H-donor (Table 3, entry 14).

Table 3

Furfural transfer hydrogenation to FA over different Zr-based catalysts.[a]

Entry	catalyst	T (°C)	furfural conversion (%)	FA yield (%)	2-FA yield (%)	FA productivity (mmol*$g^{-1}h^{-1}$)
1	ZrH	140	72	67	5	4.0
2	mZrH	140	81	77	4	4.6
3	mZrH	150	84	80	4	4.8
4	2% Ru/mZrH	140	82	79	3	4.7
5	4% Ru/mZrH	140	85	82	2	4.9
6	4% Ru/mZrH	150	88	87	1	5.2
7	6% Ru/mZrH	140	86	84	2	5.0
8	6% Ru/mZrH	150	92	91	1	5.5
9[b]	6% Ru/mZrH	150	97	96	1	3.8
10	6% $RuCl_3$/mZrH	150	82	76	3	4.6
11	6% Ru/ZrH	140	82	80	2	4.8
12	6% Ru/ZrH	150	85	84	1	5.0
13	ZrH[41]	150	59	39	-	2.5
14[c]	ZrH[41]	150	96	92	-	5.9
15	ZrO_2[41]	150	63	8	-	0.5
16[d]	$ZrO(OH)_2$[40]	150	94	84	-	2.7

[a] 0.2 M Furfural, 20 bar dynamic pressure, 0.6 g catalyst and 0.3 mL min^{-1} flow rate.
[b] 0.9 g catalyst was used.
[c] iso-propanol was used as solvent.
[d] HMF was used as starting material.
Entries 1-12 were performed in continuous flow, and entries 13-16 in batch.

With the most active catalyst 6% Ru/mZrH, we next investigated the effect of different primary alcohols on the furfural transfer hydrogenation (Table 4). The

reaction conditions were set the same with initial conditions, except for the temperature (150 ºC instead of 140 ºC). The results showed that ethanol is the most ideal primary alcohol for furfural transfer hydrogenation to FA. Furfural conversion decreased from 92 % with ethanol to 69 % with 1-butanol, but the selectivity of FA kept ~99 %. Methanol gave the poorest furfural conversion of 53 % with 91 % of FA selectivity, and the major byproduct was 2-(dimethoxymethyl)furan which means methanol is easier to form acetal with furfural than other primary alcohols.

Table 4

Furfural transfer hydrogenation with different primary alcohols.[a]

Entry	Solvent	Furfural conversion (%)	FA yield (%)	FA selectivity (%)
1	methanol	53	48	91
2	ethanol	92	91	99
3	1-propanol	83	82	99
4	1-butanol	69	68	99

[a]Reaction conditions: 150 ºC, 20 bar dynamic pressure, 0.2 M furfural, 6% Ru/mZrH (0.6 g) and 0.3 mL min^{-1} flow rate.

The stability is regarded as very important property for any heterogeneous catalyst (Fig. 5). In order to understand the effect of modification on the catalyst stability, the long-term stability study of 6 % Ru/mZrH and 6% Ru/ZrH was done. 6 % Ru/mZrH showed a more outstanding catalytic activity than 6 % Ru/ZrH, and both catalysts were stable at first 90 min, but then furfural conversion severely decreased with 6% Ru/ZrH, and the conversion of furfural reached 70 % after 300 min. However, 6 % Ru/mZrH exhibited an improved stability as furfural conversion gradually decreased only 7 % without loss of selectivity, and the conversion of furfural was 84 % after 300 min which is better than that obtained with mZrH at 150 ºC (Table 3, entry 3). The unchanged FA selectivity indicated than Ru species is still in the catalysts, even EDS

showed that little amount of Ru was leached. This might partially attribute to the decrease of furfural conversion, and the catalyst surface area reduction due to the deposition of side-products should be also responsible for the activity decrease.

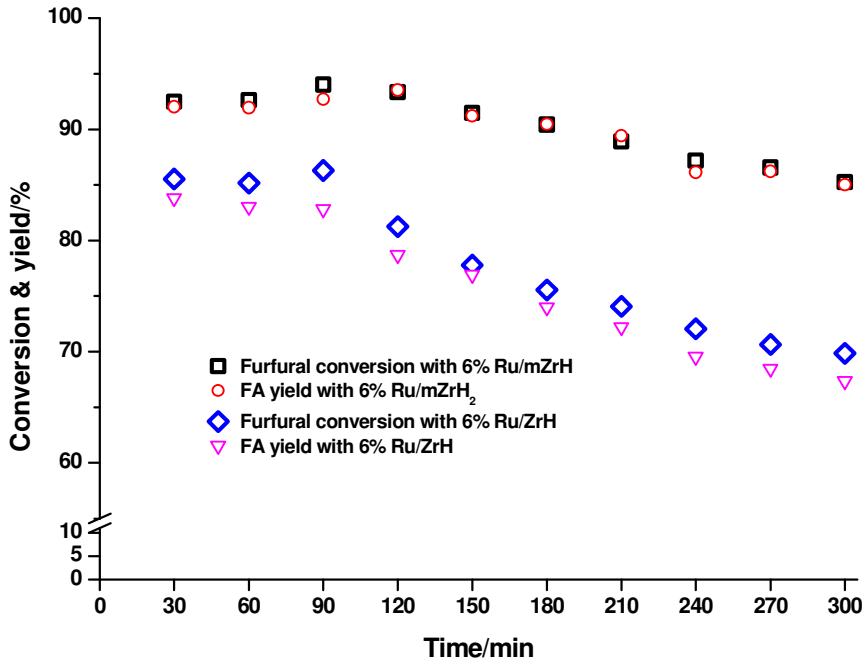

Fig. 5. Long-term stability study of 6 % Ru/mZrH and 6% Ru/ZrH. Reaction conditions: 150 ºC, 0.2 M Furfural, 20 bar dynamic pressure, catalyst (0.6 g) and 0.3 mL min^{-1} flow rate.

4. Conclusions

In summary, we have successfully developed a method for the modification of ZrH, which significantly changed its morphology and basic sites, and the modified ZrH presented an improved catalytic transfer hydrogenation performance than ZrH. The best FA yield of 91% was achieved over 6% Ru/mZrH with ethanol as both H-donor and solvent in continuous flow. Benefitted from the modification, 6% Ru/mZrH

exhibited superior catalytic performances and stability than 6% Ru/ZrH, and the deactivation of the catalysts were due to the leaching of Ru and the deposition of side-products on their surfaces. Despite these findings, more efforts should be devoted in future to illuminate the structure of mZrH in detail (CO_2 adsorption made it quite complicated).

Acknowledgements

Y.W. and D.Z. would like to thank the China Scholarship Council (CSC) for the financial support.

Appendix A. Supplementary data

The Supporting Information is available:

References

[1] M. Alberto, A.S. Roger, Utilisation of biomass for fuels and chemicals: The road to sustainability, Catal. Today 167 (2011) 1-2. DOI: 10.1016/j.cattod.2011.03.012

[2] A. Halilu, T.H. Ali, A.Y. Atta, P. Sudarsanam, S.K. Bhargava, S.B. Abd Hamid, Highly selective hydrogenation of biomass-derived furfural into furfuryl alcohol using a novel magnetic nanoparticles catalyst, Energy Fuels 30 (2016) 2216–2226. DOI: 10.1021/acs.energyfuels.5b02826

[3] T. Su, D. Zhao, M. Khodadadi, C. Len, Lignocellulosic biomass for bioethanol: recent advances, technolgy trends, and barriers to industrial development, Curr. Opin. Green Sustain. Chem. 24 (2020 56-60. DOI: 10.1016/j.cogsc.2020.04.005

[4] F. Delbecq, Y. Wang, A. Muralidhara, K. El Ouardi, G. Marlair, C. Len, Hydrolysis of hemicellulose and derivatives—A review of recent advances in

the production of furfural, Front. Chem. 6 (2018) 146. DOI: 10.3389/fchem.2018.00146

[5] S.J. Oh, S.H. Jung, J.S. Kim, Co-production of furfural and acetic acid from corncob using $ZnCl_2$ through fast pyrolysis in a fluidized bed reactor, Bioresour. Technol. 144 (2013) 172–178. DOI: 10.1016/j.biortech.2013.06.077

[6] M. Besson, P. Gallezot, C. Pinel, Conversion of biomass into chemicals over metal catalysts, Chem. Rev. 114 (2014) 1827-1870. DOI: 10.1021/cr4002269

[7] M. Hronec, K. Fulajtarová, T. Liptaj, Effect of catalyst and solvent on the furan ring rearrangement to cyclopentanone, Appl. Catal. A: General 437-438 (2012) 104-111. DOI: 10.1016/j.apcata.2012.06.018

[8] R. Mariscal, P. Maireles-Torres, M. Ojeda, I. Sádaba, M.L. Granados, Furfural: a renewable and versatile platform molecule for the synthesis of chemicals and fuels, Energy Environ. Sci. 9 (2016) 1144–1189. DOI: 10.1039/C5EE02666K

[9] K. Yan, G. Wu, T. Lafleur, C. Jarvis, Production, properties and catalytic hydrogenation of furfural to fuel additives and value-added chemicals, Renew. Sustain. Energy Rev. 38 (2014) 663–676. DOI: 10.1016/j.rser.2014.07.003

[10] C. Pischetola, L. Collado, R. Aguado-Molina, S. Martin-Treceno, M.A. Keane, F. Cardenas-Lizana, Continuous furfuryl alcohol production via coupled dehydrogenation-hydrogenation over supported Cu and Au catalysts: a consideration of hydrogen generation and transfer, Mol. Catal. 492 (2020, 110912. DOI: 10.1016/j.mcat.2020.110912

[11] M.S. Tiwari, J.S. Dicks, J. Keogh, V.V. Ranade, H.G. Manyar, Direct conversion of furfuryl alcohol to butyl levulinate using tin exchanged tungstophosphoric acid catalysts, Mol. Catal. 488 (2020) 110918. DOI: 10.1016/j.mcat.2020.110918

[12] K. Dussan, B. Girisuta, M. Lopes, J. Leahy, M. Hayes, Conversion of hemicellulose sugars catalyzed by formic acid: kinetics of the dehydration of D‐xylose, L‐arabinose, and D‐glucose, ChemSusChem. 8 (2015) 1411-1428. DOI: 10.1002/cssc.201403328

[13] B.M. Nagaraja, V. Siva Kumar, V. Shasikala, A.H. Padmasri, B. Sreedhar, B. David Raju, K.S. Rama Rao, A highly efficient Cu/MgO catalyst for vapour phase hydrogenation of furfural to furfuryl alcohol, Catal. Commun. 4 (2003) 287–293. DOI: 10.1016/S1566-7367(03)00060-8

[14] M. Lesiak, M. Binczarski, S. Karski, W. Maniukiewicz, J. Rogowski, E. Szubiakiewicz, J. Berlowska, P. Dziugan, I. Witońska, Hydrogenation of furfural over Pd–Cu/Al_2O_3 catalysts. The role of interaction between palladium and copper on determining catalytic properties, J. Mol. Catal. A: Chemical 395 (2014) 337–348. DOI: 10.1016/j.molcata.2014.08.041

[15] B.M. Nagaraja, A.H. Padmasri, B. David Raju, K.S. Rama Rao, Vapor phase selective hydrogenation of furfural to furfuryl alcohol over Cu–MgO coprecipitated catalysts, J. Mol. Catal. A: Chemical 265 (2007) 90–97. DOI: 10.1016/j.molcata.2006.09.037

[16] A. Corma, S. Iborra, A. Velty, Chemical routes for the transformation of biomass into chemicals, Chem. Rev. 107 (2007) 2411-2502. DOI: 10.1021/cr050989d

[17] M.M. Villaverde, N.M. Bertero, T.F. Garetto, A.J. Marchi, Selective liquid-phase hydrogenation of furfural to furfuryl alcohol over Cu-based catalysts, Catal. Today 213 (2013) 87–92. DOI: 10.1016/j.cattod.2013.02.031

[18] D. Liu, D. Zemlyanov, T. Wu, R.J. Lobo-Lapidus, J.A. Dumesic, J.T. Miller, C.L. Marshall, Deactivation mechanistic studies of copper chromite catalyst for

selective hydrogenation of 2-furfuraldehyde, J. Catal. 288 (2013) 336–345. DOI: 10.1016/j.jcat.2012.10.026

[19] R. Rao, A. Dandekar, R.T.K. Baker, M.A. Vannice, Properties of copper chromite catalysts in hydrogenation reactions. J. Catal. 171 (1997) 406–419. DOI: 10.1006/jcat.1997.1832

[20] M. Li, Y. Hao, F. Cárdenas-Lizana, M.A. Keane, Selective production of furfuryl alcohol via gas phase hydrogenation of furfural over Au/Al_2O_3, Catal. Commun. 69 (2015) 119–122. DOI: 10.1016/j.catcom.2015.06.007

[21] Q. Yuan, D. Zhang, L. van Haandel, F. Ye, T. Xue, E.J.M. Hensen, Y. Guan, Selective liquid phase hydrogenation of furfural to furfuryl alcohol by Ru/Zr-MOFs, J. Mol. Catal. A: Chemical 406 (2015) 58–64. DOI: 10.1016/j.molcata.2015.05.015

[22] J. Yang, J. Ma, Q. Yuan, P. Zhang, Y. Guan, Selective hydrogenation of furfural on Ru/Al-MIL-53: a comparative study on the effect of aromatic and aliphatic organic linkers, RSC Adv. 6 (2016) 92299–92304. DOI: 10.1016/j.molcata.2015.05.015

[23] J.M. Tukacs, M. Bohus, G. Dibó, L.T. Mika, Ruthenium-catalyzed solvent-free conversion of furfural to furfuryl alcohol, RSC Adv. 7 (2017) 3331–3335. DOI: 10.1039/C6RA24723G

[24] L. Liu, H. Lou, M. Chen, Selective hydrogenation of furfural over Pt based and Pd based bimetallic catalysts supported on modified multiwalled carbon nanotubes (MWNT), Appl. Catal. A: General 550 (2018) 1–10. DOI: 10.1016/j.apcata.2017.10.003

[25] K. An, N. Musselwhite, G. Kennedy, V.V. Pushkarev, L. Robert Baker, G.A. Somorjai, Preparation of mesoporous oxides and their support effects on Pt

nanoparticle catalysts in catalytic hydrogenation of furfural, J. Colloid Interface Sci. 392 (2013) 122–128. DOI: 10.1016/j.jcis.2012.10.029

[26] J. Kijeński, P. Winiarek, T. Paryjczak, A. Lewicki, A. Mikołajska, Platinum deposited on monolayer supports in selective hydrogenation of furfural to furfuryl alcohol, Appl. Catal. A: General 233 (2002) 171–182. DOI: 10.1016/S0926-860X(02)00140-0

[27] S. Nishimura, T. Shimura, K. Ebitani, Transfer hydrogenation of furaldehydes with sodium phosphinate as a hydrogen source using Pd-supported alumina catalyst, J. Taiwan Inst. Chem. E. 79 (2017) 97–102. DOI: 10.1016/j.jtice.2017.03.028

[28] R. Huang, Q. Cui, Q. Yuan, H. Wu, Y. Guan, P. Wu, Total hydrogenation of furfural over Pd/Al_2O_3 and Ru/ZrO_2 mixture under mild conditions: essential role of tetrahydrofurfural as an intermediate and support effect, ACS Sustainable Chem. Eng. 6 (2018) 6957–6964. DOI: 10.1021/acssuschemeng.8b00801

[29] S.M. Rogers, C.R.A. Catlow, C.E. Chan-Thaw, A. Chutia, N. Jian, R.E. Palmer, M. Perdjon, A. Thetford, N. Dimitratos, A. Villa, P.P. Wells, Tandem site- and size-controlled Pd nanoparticles for the directed hydrogenation of furfural, ACS Catal. 7 (2017) 2266–2274. DOI: 10.1021/acscatal.6b03190

[30] C. Nguyen-Huy, J.S. Kim, S. Yoon, E. Yang, J.H. Kwak, M.S. Lee, K. An, Supported Pd nanoparticle catalysts with high activities and selectivities in liquid-phase furfural hydrogenation, Fuel 226 (2018) 607–617. DOI: 10.1016/j.fuel.2018.04.029

[31] J. Wu, Y. Shen, C. Liu, H. Wang, C. Geng, Z. Zhang, Vapor phase hydrogenation of furfural to furfuryl alcohol over environmentally friendly Cu–

Ca/SiO_2 catalyst, Catal. Commun. 6 (2005) 633–637. DOI: 10.1016/j.catcom.2005.06.009

[32] M.A. Jackson, M.G. White, R.T. Haasch, S.C. Peterson, J.A. Blackburn, Hydrogenation of furfural at the dynamic Cu surface of $CuOCeO_2/Al_2O_3$ in a vapor phase packed bed reactor, Mol. Catal. 445 (2020) 124-132. DOI: 10.1016/j.mcat.2017.11.023

[33] T.P. Sulmonetti, S.H. Pang, M.T. Claure, S. Lee, D.A. Cullen, P.K. Agrawal, C.W. Jones, Vapor phase hydrogenation of furfural over nickel mixed metal oxide catalysts derived from layered double hydroxides, Appl. Catal. A: General 517 (2016), 187–195. DOI: 10.1016/j.apcata.2016.03.005

[34] S.-P. Lee, Y.-W. Chen, Selective hydrogenation of furfural on Ni–P, Ni–B, and Ni–P–B ultrafine materials, Ind. Eng. Chem. Res. 38 (1999) 2548–2556. DOI: 10.1021/ie990071a

[35] H. Jeong, C. Kim, S. Yang, H. Lee, Selective hydrogenation of furanic aldehydes using Ni nanoparticle catalysts capped with organic molecules, J. Catal. 344 (2016) 609–615. DOI: 10.1016/j.jcat.2016.11.002

[36] M. Manikandan, A.K. Venugopal, K. Prabu, R.K. Jha, R. Thirumalaiswamy, Role of surface synergistic effect on the performance of Ni-based hydrotalcite catalyst for highly efficient hydrogenation of furfural, J. Mol. Catal. A: Chemical 417 (2016) 153–162. DOI: 10.1016/j.molcata.2016.03.019

[37] X. Chen, H. Li, H. Luo, M. Qiao, Liquid phase hydrogenation of furfural to furfuryl alcohol over Mo-doped Co-B amorphous alloy catalysts, Appl. Catal. A: General 233 (2002) 13–20. DOI:10.1016/S0926-860X(02)00127-8

[38] R. Rodiansono, M.D. Astuti, D.R. Mujiyanti, U.T. Santoso, S. Shimazu, Novel preparation method of bimetallic Ni-In alloy catalysts supported on amorphous

alumina for the highly selective hydrogenation of furfural, Mol. Catal. 445 (2018) 52-60.

[39] C. Ramirez-Barria, M. Isaacs, K. Wilson, A. Guerrero-Ruiz, I. Rodríguez-Ramos, Optimization of ruthenium based catalysts for the aqueous phase hydrogenation of furfural to furfuryl alcohol, Appl. Catal. A: General 563 (2018) 177–184. DOI: 10.1016/j.apcata.2018.07.010

[40] H. Chen, H. Ruan, X. Lu, J. Fu, T. Langrish, X. Lu, Efficient catalytic transfer hydrogenation of furfural to furfuryl alcohol in near-critical isopropanol over Cu/MgO-Al_2O_3 catalyst, Mol. Catal. 445 (2018) 94–101. DOI: 10.1016/j.mcat.2017.11.011

[41] M.M. Villaverde, T.F. Garetto, A.J. Marchi, Liquid-phase transfer hydrogenation of furfural to furfuryl alcohol on Cu–Mg–Al catalysts, Catal. Commun. 58 (2015) 6–10. DOI: 10.1016/j.catcom.2014.08.021

[42] H. Chen, H. Ruan, X. Lu, J. Fu, T. Langrish, X. Lu, Efficient catalytic transfer hydrogenation of furfural to furfuryl alcohol in near-critical isopropanol over Cu/MgO-Al_2O_3 catalyst, Mol. Catal. 445 (2018) 94-101. DOI: 10.1016/j.mcat.2017.11.011

[43] W. Gong, C. Chen, Y. Zhang, H. Zhou, H. Wang, H. Zhang, Y. Zhang, G. Wang, H. Zhao, Efficient synthesis of furfuryl alcohol from H_2-hydrogenation/transfer hydrogenation of furfural using sulfonate group modified Cu catalyst, ACS Sustainable Chem. Eng. 5 (2017) 2172–2180. DOI: 10.1021/acssuschemeng.6b02343

[44] R. López-Asensio, J.A. Cecilia, C.P. Jiménez-Gómez, C. García-Sancho, R. Moreno-Tost, P. Maireles-Torres, Selective production of furfuryl alcohol from

furfural by catalytic transfer hydrogenation over commercial aluminas, Appl. Catal. A: General 556 (2018) 1–9. DOI: 10.1016/j.apcata.2018.02.022

[45] F. Wang, Z. Zhang, Catalytic transfer hydrogenation of furfural into furfuryl alcohol over magnetic γ-Fe_2O_3@HAP catalyst, ACS Sustainable Chem. Eng. 5 (2017) 942–947. DOI: 10.1021/acssuschemeng.6b02272

[46] W. Hao, W. Li, X. Tang, X. Zeng, U. Suna, S. Liu, L. Lin, Catalytic transfer hydrogenation of biomass-derived 5-hydroxymethyl furfural to the building block 2,5-bishydroxymethyl furan. Green Chem. 18 (2016) 1080-1088. DOI: 10.1039/C5GC01221J

[47] J. Zhang, K. Dong, W. Luo, H. Guan, Selective transfer hydrogenation of furfural into furfuryl alcohol on Zr-containing catalysts using lower alcohols as hydrogen donors, ACS Omega 3 (2018) 6206–6216. DOI: 10.1021/acsomega.8b00138

[48] M.N. Hughes, K. Shrimanker, Metal complexes of hydroxylamine, Inorg. Chim. Acta 18 (1976) 69-76. DOI: 10.1016/S0020-1693(00)95587-7

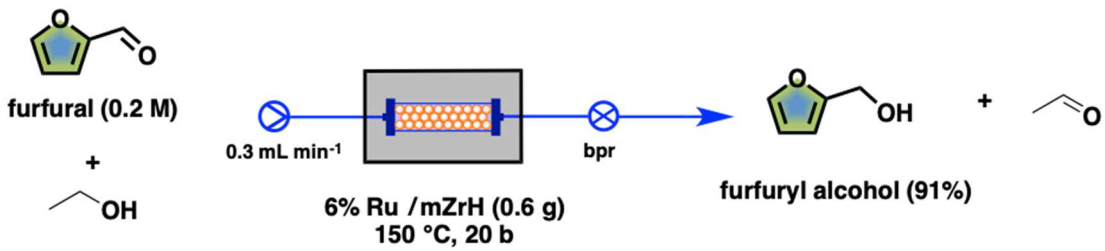
furfural (0.2 M)
+
OH
0.3 mL min-1
6% Ru /mZrH (0.6 g)
150 °C, 20 b
bpr
OH
+
furfuryl alcohol (91%)